

# A hybrid three-dimensional electromagnetic modeling scheme

K. H. Lee\*, D. F. Pridmore‡, and H. F. Morrison\*

## ABSTRACT

We present an efficient numerical method for computing electromagnetic (EM) scattering of arbitrary three-dimensional (3-D) local inhomogeneities buried in a uniform or two-layered earth.

In this scheme the inhomogeneity is enclosed by a volume whose conductivity is discretized by a finite-element mesh and whose boundary is only a slight distance away from the inhomogeneity. The scheme uses two sets of independent equations. The first is a set of finite-element equations derived from a variational integral, and the second is a mathematical expression for the fields at the boundary in terms of electric fields inside the boundary. The Green's function is used to derive the second set of equations. An iterative algorithm has been developed to solve these two sets of equations. The solutions are the electric fields at nodes inside the finite-element mesh. The scattered fields anywhere may then be obtained by performing volume integrations over the inhomogeneous region.

The scheme is used for modeling 3-D inhomogeneities with plane-wave and magnetic dipole sources. The results agree with earlier model analyses using the finite-element technique.

## INTRODUCTION

A limited number of numerical solutions for three-dimensional (3-D) electromagnetic (EM) problems have been discussed in the geophysical literature. These solutions have been obtained using the integral equation, finite-element, or finite-difference techniques. Lines and Jones (1973) and Reddy et al (1977) presented solutions to 3-D magnetotelluric (MT) problems using finite-difference and finite-element techniques, respectively. Pridmore (1978) reported iterative solutions to 3-D electric and EM problems using the finite-element technique. The drawbacks of these techniques are: (1) the number of equations is so large that the computer cost is prohibitive, and (2) numerical differentiation of the obtained solution, which is necessary to compute the full set of fields, is not always reliable. The difficulties can be avoided by using the integral equation technique provided the inhomogeneity is of finite extent. The application of the integral equation technique to 3-D EM problems was reported by Hohmann (1975), Weidelt (1975), and Meyer (1977). In this technique, the number

of equations is basically the same as the number of inhomogeneous elements, but the matrix is full and generally asymmetric.

A hybrid scheme, which uses a combination of these techniques, was introduced by Scheen (1978). A variational integral for the magnetic field is initially formulated over a region discretized by a finite-element mesh, and a system of linear equations is derived from the variational integral. Then, using integral relations, a second set of equations is derived for the scattered magnetic fields at the mesh boundary positioned some distance away from the inhomogeneity. To derive the second set of equations, the scattering current must first be found through a numerical  $\nabla \times \mathbf{H}$  operation. An algebraic substitution of the second set of equations into the first set leads to a combined set of linear equations, from which magnetic fields inside the finite-element mesh are finally obtained. This is the direct hybrid scheme. The matrix for the combined set of equations is full and asymmetric. The size of the matrix is slightly larger than the one associated with the integral equation technique, but the scheme does not need to evaluate Green's functions between elements within the finite-element mesh, thus avoiding the problem of singular cell integration. The second approach discussed by Scheen is an iterative scheme which uses the same sets of equations. Initial field values are assigned along the boundary, and the first set of finite-element equations is solved. Scattered magnetic fields are then calculated using the second set of equations. These scattered fields are substituted for the boundary fields and the process is repeated iteratively until changes in the boundary values become insignificant.

In the present approach, we have solved the problem iteratively in terms of the secondary electric fields within the mesh. The scattering currents can then be obtained directly by adding appropriate primary electric fields to the finite-element solutions and by multiplying the results by the anomalous conductivities. This process avoids the difficulty of taking the numerical curl operation, which would otherwise be necessary when the solution is derived in terms of magnetic fields.

## FORMULATIONS OF FINITE-ELEMENT EQUATIONS AND INTEGRAL RELATIONS

We first derive a set of finite-element equations from a variational integral. The variational integral may be formulated using either the total EM energy contained in the system (Morse and Feshbach, 1953) or a mathematical function defined by the minimum theorem (Stakgold, 1968). In order to apply the minimum theorem, it is necessary to introduce a stationary principle to derive the finite-element equations.

Manuscript received by the Editor February 29, 1980; revised manuscript received August 11, 1980.

\*Hearst Mining Building, Room 414, University of California, Berkeley, CA 94720.

‡Western Mining Corp., 55 McDonald Street, Kalgoorlie, W. A. 6430, Australia.

0016-8033/81/0501-796\$03.00. © 1981 Society of Exploration Geophysicists. All rights reserved.

Maxwell's equations for an  $e^{j\omega t}$  time dependent system become

$$\nabla \times \mathbf{E} = -\hat{z}\mathbf{H} - \mathbf{M}_s, \quad (1)$$

and

$$\nabla \times \mathbf{H} = \hat{y}\mathbf{E} + \mathbf{J}_s \quad (2)$$

where  $\hat{z} = j\omega\mu$  and  $\hat{y} = \sigma + j\omega\epsilon$ , and  $\mathbf{M}_s$  and  $\mathbf{J}_s$  are impressed magnetic and electric sources. The domain equation for the electric field in the presence of  $\mathbf{J}_s$  alone is derived from equations (1) and (2) as

$$\nabla \times \frac{\nabla \times \mathbf{E}}{\hat{z}} + \hat{y}\mathbf{E} = -\mathbf{J}_s. \quad (3)$$

If we generalize the inner product to include the one with no complex conjugation of one of the vectors involved, the minimum theorem provides the corresponding functional to equation (3) as

$$F(\mathbf{E}) = \int_v \left[ \left( \nabla \times \frac{\nabla \times \mathbf{E}}{\hat{z}} + \hat{y}\mathbf{E} \right) \cdot \mathbf{E} + 2\mathbf{E} \cdot \mathbf{J}_s \right] dv. \quad (4)$$

This is not the usual inner product defined in complex space. Under this inner product, the operator  $[\nabla \times (\nabla \times \mathbf{E})/\hat{z} + \hat{y}]$  is self-adjoint under homogeneous Dirichlet and natural boundary conditions, but not positive definite. Since the operator is not positive definite, the minimum theorem does not hold. However, it can be shown (Pridmore, 1978) that the solution to equation (3) corresponds to a stationary point of the functional  $F(\mathbf{E})$ . Applying the vector identity,  $\nabla \cdot \mathbf{A} \times \mathbf{B} = \mathbf{B} \cdot \nabla \times \mathbf{A} - \mathbf{A} \cdot \nabla \times \mathbf{B}$ , and the divergence theorem, equation (4) becomes

$$\sum_i \left[ \int_{v_i} \left( \frac{\nabla \times \mathbf{E} \cdot \nabla \times \mathbf{E}}{\hat{z}} + \hat{y}\mathbf{E} \cdot \mathbf{E} + 2\mathbf{E} \cdot \mathbf{J}_s \right) dv + \int_{s_i} (\mathbf{E} \times \mathbf{H}) \cdot d\mathbf{s} \right], \quad (5)$$

where the volume has been divided into a number of smaller ones over which  $\sigma$  is constant. The surface integrals along adjacent boundaries must cancel because the tangential components of  $\mathbf{E}$  and  $\mathbf{H}$  are continuous. At the external boundary, the surface integrals will not contribute to the variation of  $F(\mathbf{E})$ . With proper boundary values, such as the tangential components of either  $\mathbf{E}$  or  $\mathbf{H}$  prescribed, the variation of  $\int_s (\mathbf{E} \times \mathbf{H}) \cdot d\mathbf{s}$  would vanish. Another useful condition commonly encountered is  $\mathbf{E} \times \mathbf{H} \cdot \mathbf{n} = 0$ , namely the natural boundary condition. If the EM fields are either symmetric or antisymmetric across a certain surface, this surface may be called a natural boundary, and no power is transmitted across this surface. Thus, the effective variational integral is the volume integral part of equation (5).

$$F(\mathbf{E}) = \sum_i \int_{v_i} \left( \frac{\nabla \times \mathbf{E} \cdot \nabla \times \mathbf{E}}{\hat{z}} + \hat{y}\mathbf{E} \cdot \mathbf{E} + 2\mathbf{E} \cdot \mathbf{J}_s \right) dv. \quad (6)$$

The functional is in terms of the total electric fields. If we know the primary electric field, the field that would exist in the presence of a horizontally layered half-space alone, the functional could alternatively be formulated in terms of the secondary electric fields. According to the principle of superposition  $\mathbf{E} = \mathbf{E}_p + \mathbf{E}_s$ , we can derive the domain equation for the secondary electric field as

$$\nabla \times \frac{\nabla \times \mathbf{E}_s}{\hat{z}} + \hat{y}\mathbf{E}_s = -\Delta\hat{y}\mathbf{E}_p. \quad (7)$$

where subscripts  $s$  and  $p$  denote secondary and primary, respectively, and  $\Delta\hat{y}$  is the difference in  $\hat{y}$  between the medium

used for the primary field calculation and the inhomogeneity. The corresponding functional  $F(\mathbf{E}_s)$  can also be written as

$$F(\mathbf{E}_s) = \sum_i \int_{v_i} \left( \frac{\nabla \times \mathbf{E}_s \cdot \nabla \times \mathbf{E}_s}{\hat{z}} + \hat{y}\mathbf{E}_s \cdot \mathbf{E}_s + 2\Delta\hat{y}\mathbf{E}_s \cdot \mathbf{E}_p \right) dv. \quad (8)$$

Using hexahedral elements and a trilinear basis function which describes the field behavior in each element, the secondary electric fields in a particular element  $e$  may be approximated by (Zienkiewicz, 1977)

$$\mathbf{E}_s^e = (N_1 N_2 \dots N_8)(\mathbf{E}_{s1} \mathbf{E}_{s2} \dots \mathbf{E}_{s8})^T$$

for each component of the electric fields. The shape functions  $N_j$ ,  $j = 1 \sim 8$ , are trilinear, and  $\mathbf{E}_{sj}$ ,  $j = 1 \sim 8$ , are the unknown secondary fields at eight corners of a hexahedron. Substituting the approximation into equation (8), carrying out volume integrations, and stacking these elementary entries into a system matrix  $\mathbf{K}$ , we obtain the following approximate matrix representation for the functional  $\tilde{F}(\mathbf{E}_s)$ :

$$\tilde{F}(\mathbf{E}_s) = \mathbf{E}_s^T \mathbf{K} \mathbf{E}_s + 2\mathbf{E}_s^T \mathbf{S}. \quad (9)$$

where  $\mathbf{S}$  is a source vector obtained from the last part of the integral (8) over the volume  $v_i$  summed over  $i$ . The stationary point of  $\tilde{F}$  can be found by setting the first derivative of  $\tilde{F}$  with respect to  $\mathbf{E}_s$  to zero. The first derivative of  $\tilde{F}$  is equivalent to the first variation of  $\tilde{F}$ . This generates the finite-element matrix equation

$$\mathbf{K} \mathbf{E}_s = -\mathbf{S}. \quad (10)$$

The system matrix  $\mathbf{K}$  is banded and symmetric. For a grid system of  $10 \times 10 \times 10$  nodes in each direction, the total number of equations is 3000 with a maximum half bandwidth of 336 including the diagonal entry. The memory requirement for this system is roughly 1 million complex words. This is about the maximum size for the iterative hybrid scheme to be economically practical.

To solve equation (10), we must determine both the primary fields inside the inhomogeneity and the secondary fields at nodes on the boundary of the finite-element mesh. The primary field solution for a layered half-space was given by Wait (1962), Quon (1963), Frischknecht (1967), Dey and Ward (1970), and Ryu et al (1970), to list a few.

To find the secondary field scattered by an inhomogeneity, let us first consider a point source of current  $\mathbf{J}^s$  in the lower half-space of a two-layered earth. Following Harrington (1961, p. 77), we write the divergenceless vector  $\mathbf{H}$  as the curl of a vector  $\mathbf{A}$ ,  $\mathbf{H} = \nabla \times \mathbf{A}$ , which satisfies the following inhomogeneous wave equation in rectangular coordinates

$$\nabla^2 \mathbf{A} + k^2 \mathbf{A} = -\mathbf{J}^s \delta(\mathbf{r} - \mathbf{r}'), \quad (11)$$

where  $k^2 = -\hat{z}\hat{y}$ , and  $\mathbf{r}$  and  $\mathbf{r}'$  are the positions of observation and source, respectively. The particular solution to equation (11) is given by

$$\mathbf{A}^p = \frac{\mathbf{J}^s}{4\pi} \frac{e^{-jk|\mathbf{r}-\mathbf{r}'|}}{|\mathbf{r}-\mathbf{r}'|}, \quad (12)$$

and the primary fields generated by the solution  $\mathbf{A}^p$  are given by

$$\mathbf{E}^p = -\hat{z}\mathbf{A}^p + \frac{1}{\hat{y}} \nabla(\nabla \cdot \mathbf{A}^p) \quad (13)$$

and

$$\mathbf{H}^p = \nabla \times \mathbf{A}^p. \quad (14)$$

In the presence of horizontal interfaces, we must consider the secondary field caused by the reflections at these boundaries.

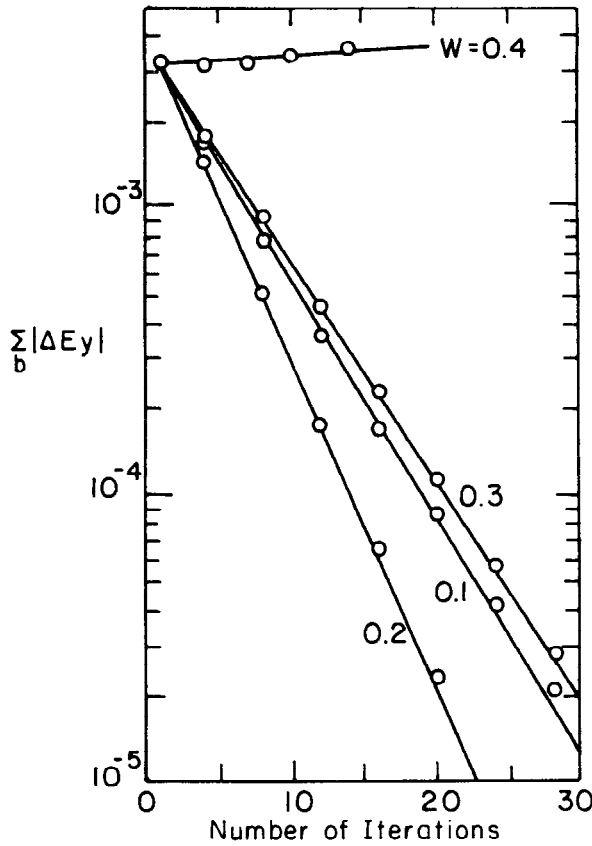


FIG. 1. Convergence diagram.

The derivation of the secondary field is given in the Appendix. In the integral equation technique, the conductive inhomogeneity is simulated by a collection of electric current sources distributed over the volume occupied by the inhomogeneity. This current is called the scattering current and is defined by the product of  $\Delta\hat{y}$  and the total electric field (Harrington, 1961). The true boundary value of the hybrid scheme is the scattered field due to the inhomogeneity. Therefore, the boundary value is the volume integral of the electric field given by equation (A-18) with  $\mathbf{J}^s(\mathbf{r}')$  replaced by  $\Delta\hat{y}(\mathbf{r}')[\mathbf{E}_p(\mathbf{r}') + \mathbf{E}_s(\mathbf{r}')]$ . Thus,

$$\mathbf{E}_s(\mathbf{r}) = \int_v \mathbf{\Gamma}^E(\mathbf{r}; \mathbf{r}') \cdot \Delta\hat{y}(\mathbf{r}')[\mathbf{E}_p(\mathbf{r}') + \mathbf{E}_s(\mathbf{r}')] dv. \quad (15)$$

Using the same grid system that gives rise to the finite-element equation (10), we can rewrite the integral (15) as

$$\mathbf{E}_s(\mathbf{r}) = \sum_i \int_{v_i} \mathbf{\Gamma}^E(\mathbf{r}; \mathbf{r}') \cdot \Delta\hat{y}(\mathbf{r}')[\mathbf{E}_p(\mathbf{r}') + \mathbf{E}_s(\mathbf{r}')] dv, \quad (16)$$

where  $\Delta\hat{y}(\mathbf{r}')$  is assumed to be a constant in each hexahedron. Then the scattered field at the boundary of the finite-element mesh may be approximated in the matrix form as

$$\mathbf{E}_s^b = \mathbf{G}\mathbf{E}_s^i + \mathbf{S}_p \quad (17)$$

where superscripts  $b$  and  $i$  denote boundary and inhomogeneous region, respectively, and  $\mathbf{S}_p$  is an additional source vector due to the primary field.  $\mathbf{G}$  is an  $m \times n$  matrix whose entries may be obtained by integrating  $\mathbf{\Gamma}^E(\mathbf{r}; \mathbf{r}') N(\mathbf{r}')$  over each elementary volume. Here,  $N(\mathbf{r}')$  is the same shape function used for the

derivation of the finite-element equation (10), and  $m$  and  $n$  are the numbers of nodal points on the boundary and inside the boundary, respectively. If we partition the finite-element equation (10) into

$$\begin{pmatrix} K_{ii} & K_{ib} \\ K_{bi} & K_{bb} \end{pmatrix} \begin{pmatrix} \mathbf{E}_s^i \\ \mathbf{E}_s^b \end{pmatrix} = - \begin{pmatrix} \mathbf{S}_i \\ \mathbf{S}_b \end{pmatrix}, \quad (18)$$

then the upper part of equation (18) is

$$K_{ii}\mathbf{E}_s^i + K_{ib}\mathbf{E}_s^b = -\mathbf{S}_i. \quad (19)$$

Substituting equation (17) into (19), we find

$$(K_{ii} + K_{ib}\mathbf{G})\mathbf{E}_s^i = -(\mathbf{S}_i + K_{ib}\mathbf{S}_p),$$

and the solution for  $\mathbf{E}_s^i$  becomes

$$\mathbf{E}_s^i = -(K_{ii} + K_{ib}\mathbf{G})^{-1}(\mathbf{S}_i + K_{ib}\mathbf{S}_p). \quad (20)$$

This is the direct hybrid scheme for the secondary electric fields inside the boundary. The matrix  $(K_{ii} + K_{ib}\mathbf{G})$  is asymmetric, full, and of order  $n$ .

The iterative hybrid scheme is initiated by solving the finite-element equation (19) using an initial guess for the boundary values. Thus, the initial secondary field solution becomes

$$\mathbf{E}_s^i = -K_{ii}^{-1}(\mathbf{S}_i + K_{ib}\mathbf{E}_s^b). \quad (21)$$

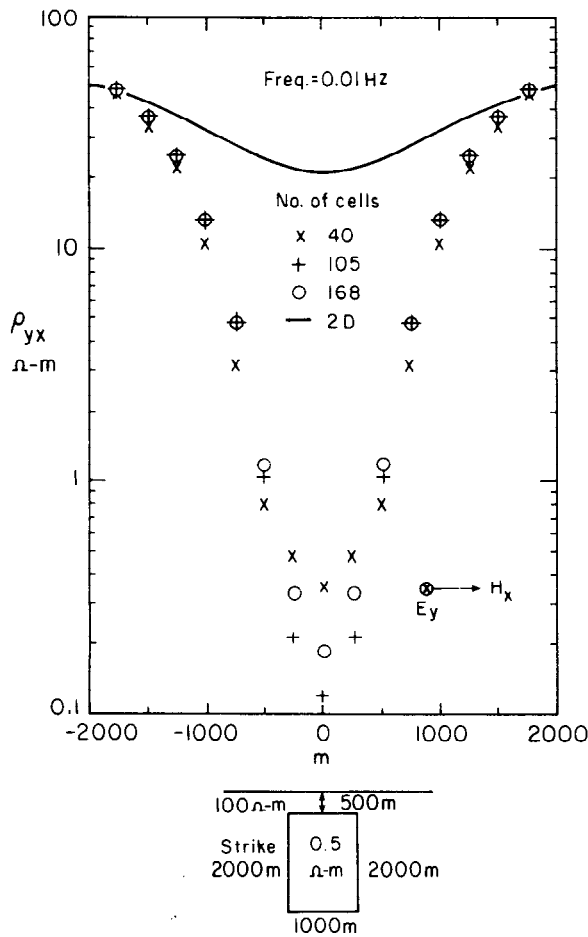
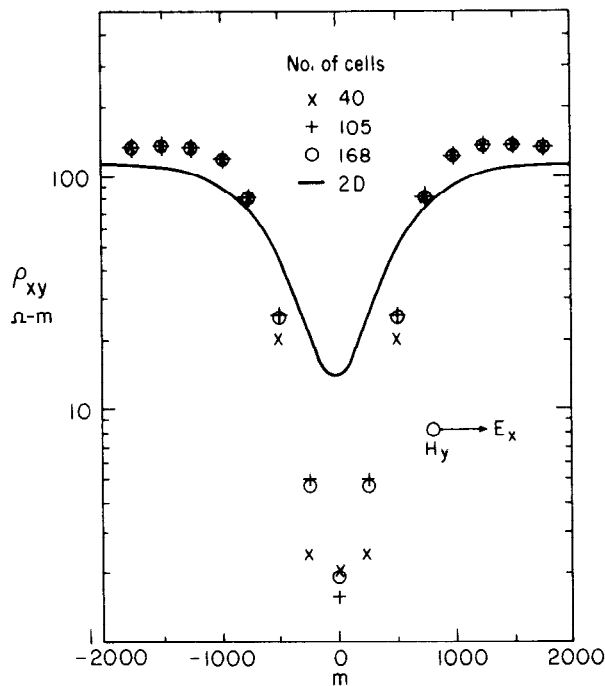
A version of a direct solution algorithm described by Reid (1972) has been used. With this initial solution inside the inhomogeneity, the scattered field is computed at the boundary using equation (17). The volume integral of Green's function is carried out using one- or two-point Gaussian quadrature. The Green's dyadics computed during the first iteration are stored and repeatedly used as the iteration is continued.

The boundary value for the  $i$ th iteration is given by

$$(\mathbf{E}_s^b)^i = (\mathbf{E}_s^b)^{i-1} + W[\mathbf{E}_s^* - (\mathbf{E}_s^b)^{i-1}], \quad (22)$$

where  $\mathbf{E}_s^*$  is the scattered field given by equation (17), and  $W$  is a weighting coefficient. A number of different values of  $W$  have been tested on a simple 3-D model. The model is a brick of size  $1 \times 2 \times 2$  km in  $x$ ,  $y$ , and  $z$ , respectively, buried at a depth of 1 km in a uniform half-space of 100  $\Omega$ -m resistivity. The resistivity of the body is 5  $\Omega$ -m, and the frequency is 1.0 Hz. The incident field is a plane wave with the electric field polarized in the  $y$ -direction. The amplitude of the incident electric field is 1.0 V/m. Figure 1 shows the sum of the absolute changes in  $E_y$  versus the number of iterations for different weighting coefficients. The sum diverges when  $W$  is 0.4, and converges fastest when it is 0.2. Since the diagram shows the sum of the absolute changes, oscillatory behavior expected for a particular field component cannot be observed. Based on the results of the test model, all the model results presented here have been obtained using a weighting coefficient of 4.0 divided by the conductivity contrast (20 for the test model) of each model. It should be mentioned that when the conductivity contrast is higher than approximately 1000, the rate of convergence is extremely slow, and may even diverge.

As an additional convergence check, a number of solutions were obtained for an MT model by changing the number of cells. The model is a conductive brick  $1 \times 2 \times 2$  km in size buried in a uniform half-space of 100  $\Omega$ -m resistivity. The depth from the surface to the top of the body is 0.5 km, and the resistivity of the body is 0.5  $\Omega$ -m. The incident field is a plane wave with the electric field polarized either in the  $y$ -direction or in the  $x$ -direction. For a frequency of 0.01 Hz, the apparent resistivity profiles obtained for each polarization have been plotted in Figures 2 and 3, respectively. Each figure contains three profiles obtained by vary-

FIG. 2. Apparent resistivity  $\rho_{yx}$  for the conductive brick model.FIG. 3. Apparent resistivity  $\rho_{xy}$  for the conductive brick model.

ing the number of cells: 40, 105, and 168. In addition, 2-D results were computed with Ryu's (1971) finite-element algorithm and plotted in the corresponding figures. The convergence is reasonable, at least for the  $E_x$ -incident case, even though the conductivity contrast of the model is relatively high.

### RESULTS AND APPLICATIONS

The EM responses of several models have been obtained with the iterative hybrid scheme. The source is a magnetic dipole on or above the surface of the earth. The required number of iterations differed from model to model, but it was between 30 and 50.

The first model consists of a 1.82 Ω-m conductor  $500 \times 3000 \times 500$  m buried in a uniform half-space of 13.7 Ω-m resistivity. The depth to the top of the body is 200 m. It corresponds to a scale tank model studied by Frischknecht (personal communication, 1975). An array of horizontal loops separated by 2000 m is moved on the surface of the earth across the top of the center of the body. The frequency is 0.15 Hz. The in-phase and quadrature parts of the normalized  $H_z$  versus the array center are plotted in Figure 4. The hybrid solution has a maximum in-phase anomaly twice as large as that of the tank model. The symmetric peaks in the quadrature response on the sides of the anomaly are not observed in the hybrid solution. An integral equation solution obtained for the same model (Meyer, 1977) also failed to show these peaks. This may indicate a limitation of available 3-D numerical techniques in general. The response of the body is due to both induction and current channeling. The current induced channels in the half-space in and out of the body as would be conduction current. In addition, an eddy current is induced in the body and tends to be concentrated near its surface. A limited number of elements simulating a 3-D body cannot accurately represent the fields associated with these induction currents. However, in analyzing

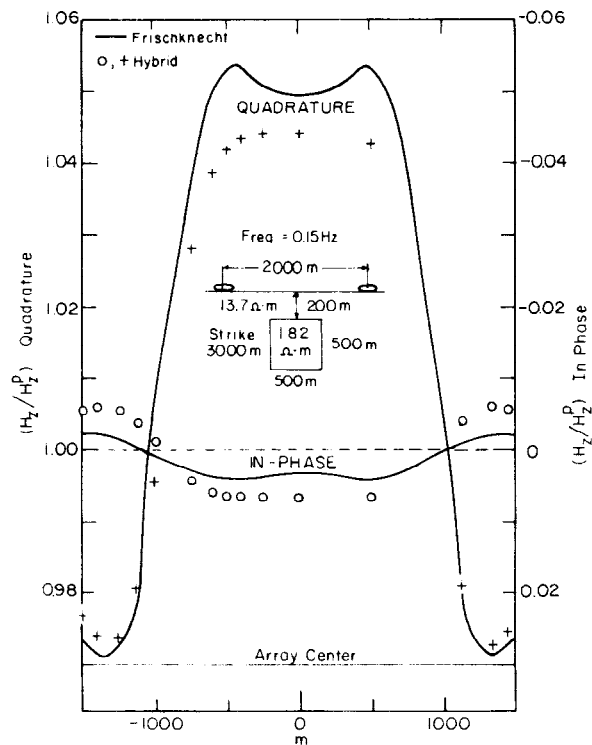


FIG. 4. Comparison between Frischknecht's scale tank model result and the hybrid solution.

field data, the numerical error shown in Figure 4 would not cause serious problems, since errors in the field data will usually be greater than the numerical errors, at least for the quadrature components.

The next model is a 1  $\Omega$ -m conductor  $30 \times 120 \times 90$  m buried at a depth of 30 m in a uniform half-space of 30  $\Omega$ -m resistivity. A vertical magnetic dipole of moment  $4\pi$  A-turn-m<sup>2</sup> is on the surface of the earth 75 m to the left of the center of the body. The frequency used is 1000 Hz. The vertical component of the secondary magnetic field  $H_z^s$  was normalized by the free space vertical magnetic field  $H_z^p$ , and the result is plotted in Figure 5. At the end of the thirtieth iteration, the average change in the boundary values became less than 0.1 percent. Along with the hybrid solution, a finite-element solution has been plotted and compared. The electric field was initially obtained using the point iterative method on a system of finite-element equations, then the magnetic field was computed using Green's functions (Pridmore, 1978). The quadrature part of  $H_z^s$  shows good agreement between the solutions; the in-phase values differ by approximately 6 percent at large separations.

The last model is a 5  $\Omega$ -m conductive brick buried in an earth of 100  $\Omega$ -m resistivity with a 25 m thick overburden layer of 30  $\Omega$ -m resistivity. The depth to the top of the body is 50 m and the size of the body is  $50 \times 250 \times 200$  m. A single coil, with its magnetic moment oriented in the  $x$ -direction, is flown 50 m above the ground across the center of the body in the direction parallel to the  $x$ -axis. The frequency is 30 Hz. The solution for this model was obtained to study the response of an airborne superconducting single coil system [Morrison, et al (1976)]. The basis of the superconducting single coil system is that the secondary field produced by a conductive half-space, with or without inhomogeneities, can be measured as the changes in input impedance  $Z$  of the transmitting coil itself. The secondary magnetic field induces a small voltage in the transmitter of

$$\Delta V = -N \frac{d}{dt} \int_s \mathbf{B} \cdot d\mathbf{s},$$

where  $N$  is the number of turns. Considering that the secondary field at the transmitter is locally uniform, and that only  $H_x$  contributes to the dot product  $\mathbf{B} \cdot d\mathbf{s}$ , the change in the voltage can be rewritten as

$$\Delta V = -j\omega\mu NAH_x,$$

where  $A$  is the cross-sectional area of the coil. Since the secondary magnetic field is proportional to the magnetic moment ( $NIA$ ) of the transmitter, the  $\Delta V$  may be computed by

$$\Delta V = -j\omega\mu(NA)^2 \bar{H}_x,$$

where  $\bar{H}_x$  is defined as the secondary  $H_x$  due to a unit magnetic moment. The change in the voltage in turn creates a change in the input impedance of the transmitter such that  $\Delta Z = \Delta R + j\omega\Delta L = \Delta V/I$ . Matching the real and imaginary parts of the  $\Delta V$  separately, we find

$$\Delta R = \omega\mu(NA)^2 \text{Im}(\bar{H}_x),$$

and

$$\Delta L = -\mu(NA)^2 \text{Re}(\bar{H}_x).$$

The plots shown in Figure 6 are the in-phase and quadrature parts of  $\bar{H}_x$  computed at the transmitter, i.e., the magnetic moment used in 1.0 A-turn-m<sup>2</sup>, or alternatively  $NA = I = 1$ . At 30 Hz, the single coil would experience a resistance change of  $3.15 \times 10^{-13} \Omega$  in moving from the background level to the peak of the

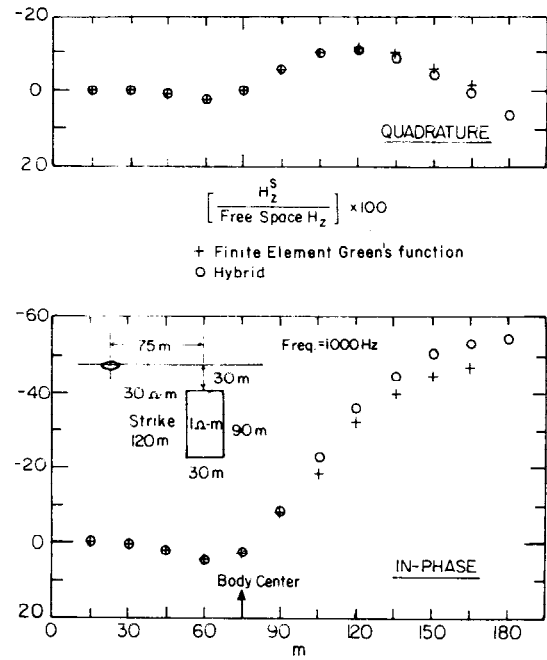


FIG. 5. Comparison of the normalized  $H_z$  between the finite-element solution and the hybrid solution for a conductive brick: data plotted at the position of the receiver coil.

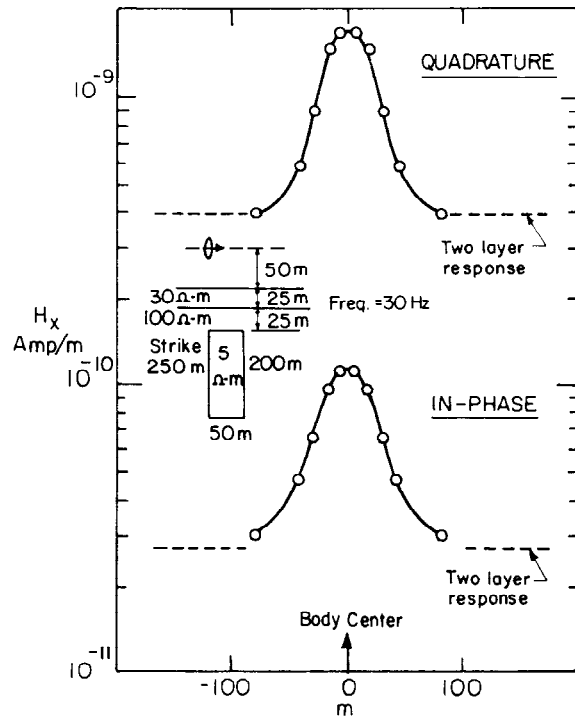


FIG. 6. Total secondary EM response in  $H_x$  measured at the center of the single coil. A conductor is buried in the lower half-space of a two-layer earth.

anomaly in less than 100 m. The change in inductance would be  $1.07 \times 10^{-17}$  H in roughly the same distance. Assuming that a superconducting coil possesses an  $(NA)^2$  of  $10^8$  and that the system is capable of detecting  $10^{-6}$   $\Omega$  with a system noise of roughly the same magnitude, the anomaly in  $\Delta R$  would be  $3.15 \times 10^{-5}$   $\Omega$ . The signal-to-noise (S/N) ratio would be approximately 30. It would be difficult, if not impossible, to measure the in-phase anomaly of  $1.07 \times 10^{-9}$  H.

### DISCUSSION OF METHODS AND CONCLUSIONS

A numerical solution for the 3-D EM problem can be obtained using either the direct or iterative hybrid scheme. The same number of Green's functions must be evaluated in either approach. For a typical iterative solution, more than half of the total CP time was spent for the evaluation of Green's functions. The iterative scheme solves a system of finite-element equations whose matrix is banded and symmetric, but it takes a considerable number of iterations to obtain a solution. Consider a finite-element mesh consisting of 20 nodes in each direction. The number of unknowns ( $n$ ) inside the boundary is 17,496, and the number of unknowns ( $m$ ) at the boundary is 6504. The maximum half bandwidth ( $l$ ) of the finite-element system matrix is 1266. The number of complex multiplications required for a direct solution would be approximately  $0.5 \times n^3$ , or  $2.68 \times 10^{12}$ , excluding the number for the evaluation of Green's functions. An iterative solution requires  $0.5 \times n \times (l + 1) \times (l + 2)$  operations for the initial decomposition of the finite-element matrix, plus  $2 \times n \times (l + 1) + 3 \times m \times n$  operations for the back substitution and boundary value computation for each iteration. The sum is roughly  $1.41 \times 10^{10} + 3.85 \times 10^8 \times N$  at the end of the  $N$ th iteration. Theoretically, the iterative scheme should be more cost effective than the direct hybrid scheme if  $N$  is less than 6900. Unfortunately, this is not the case in practice. Use of extended memory (disk) forces the iterative scheme to be severely I/O bound, and consequently the advantage of the scheme becomes much smaller than expected. The typical CP to I/O ratio for the iterative scheme was 0.2 on the CDC 7600 computer. The results obtained for the Frischknecht model (Figure 4), as an example, cost approximately \$200, of which less than \$35 was actually spent on the computation.

In the direct hybrid scheme, the boundary values are initially expressed in terms of the internal unknowns using an integral relation and then substituted into the finite-element equations resulting in a set of combined equations. The solutions to these combined equations are the fields inside the finite-element boundary.

Some analysis shows that a more cost effective direct hybrid scheme can be formulated easily. Substituting the internal unknowns  $\mathbf{E}_s^i$  [equation (21)] into equation (17), we obtain

$$\mathbf{E}_s^b = -\mathbf{G}\mathbf{K}_{ii}^{-1}(\mathbf{K}_{ib}\mathbf{E}_s^b + \mathbf{S}_i) + \mathbf{S}_p. \quad (23)$$

Then the direct solution for the boundary value  $\mathbf{E}_s^b$  becomes

$$\mathbf{E}_s^b = (\mathbf{I}_m + \mathbf{G}\mathbf{K}_{ii}^{-1}\mathbf{K}_{ib})^{-1}(\mathbf{S}_p - \mathbf{G}\mathbf{K}_{ii}^{-1}\mathbf{S}_i), \quad (24)$$

where  $\mathbf{I}_m$  is an  $m \times m$  identity matrix. The scattered fields elsewhere can then be obtained by initially calculating the fields inside the boundary using equation (21) and then carrying out necessary volume integrations. In terms of the number of operations, the ratio of the direct hybrid scheme [equation (20)] to the one whose boundary value is given by equation (24), would be roughly  $(n/m)^3$ . Depending upon the ratio  $(n/m)$  of a given model, a substantial amount of computing time could be saved. For the same mesh described earlier in this section, the ratio  $(n/m)^3$  would be approximately 19, a saving of at least a factor of 10.

### ACKNOWLEDGMENTS

This research was supported by a grant from Amax Exploration, Inc. The computer modeling was supported in part by the U.S. Dept. of Energy, Division of Geothermal Energy under contract W-7405-ENG-48 to the Lawrence Berkeley Laboratory and the University of California, Berkeley.

The authors would like to acknowledge Dr. William Scheen of Royal Dutch Shell for bringing this concept to our attention in a lecture at the Electromagnetic Workshop held at the Lawrence Berkeley Laboratory in 1978.

### REFERENCES

- Banos, A., 1966, Dipole radiation in the presence of a conducting half-space: New York, Pergamon Press.
- Dey, A., and Ward, S. H., 1970, Inductive soundings of a layered earth with a horizontal magnetic dipole: *Geophysics*, v. 35, p. 660.
- Frischknecht, F. C., 1967, Fields about an oscillating magnetic dipole over a two-layer earth, and application to ground and airborne electromagnetic surveys: *Colorado School of Mines Quart.*, v. 62, no. 1.
- Harrington, R. F., 1961, Time-harmonic electromagnetic fields: New York, McGraw-Hill Book Co., Inc.
- Hohmann, G. W., 1975, Three-dimensional induced polarization and electromagnetic modeling: *Geophysics*, v. 40, p. 309-324.
- Lines, L. R., and Jones, F. W., 1973, The perturbation of alternating geomagnetic fields by three-dimensional island structures: *Geophys. J. Roy. Astr. Soc.*, v. 32, p. 133-154.
- Meyer, W. H., 1977, Computer modeling of electromagnetic prospecting methods: University of California, Berkeley, Ph.D. thesis.
- Morrison, H. F., Dolan, W., and Dey, A., 1976, Earth conductivity determinations employing a single superconducting coil: *Geophysics*, v. 41, p. 1184-1206.
- Morse, P. M., and Feshbach, H., 1953, Methods of theoretical physics: New York, McGraw-Hill Book Co., Inc.
- Pridmore, D. F., 1978, Three-dimensional modeling of electric and electromagnetic data using the finite-element method: Ph.D. thesis, University of Utah.
- Quon, C., 1963, Electromagnetic fields of elevated dipoles on a two-layer earth: M.S. thesis, University of Alberta.
- Reddy, I. K., Rankin, D., and Phillips, R. J., 1977, Three-dimensional modeling in magnetotelluric and magnetic variational sounding: *Geophys. J. Roy. Astr. Soc.*, v. 51, p. 313-326.
- Reid, J. K., 1972, Two Fortran subroutines for direct solution of linear equations whose matrix is sparse, symmetric, and positive-definite: U.K.A.E.A. Res. Group Rep. AERE-R7119.
- Ryu, J., 1971, Low frequency electromagnetic scattering: Ph.D. thesis, University of California, Berkeley.
- Ryu, J., Morrison, H. F., and Ward, S. H., 1970, Electromagnetic fields about a loop source of current: *Geophysics*, v. 35, p. 862.
- Scheen, W. L., 1978, EMMMA, a computer program for three-dimensional modeling of airborne electromagnetic surveys: Proc., workshop on modeling of electrical and electromagnetic methods, LBL-7053, p. 53.
- Stakgold, I., 1968, Boundary value problems of mathematical physics, v. II: New York, Macmillan.
- Wait, J. R., 1962, Electromagnetic waves in stratified media: New York, Macmillan.
- Weidelt, P., 1975, Electromagnetic induction in three-dimensional structures: *J. Geophysics*, v. 41, p. 85-109.
- Zienkiewicz, O. C., 1977, The finite element method in engineering science: New York, McGraw-Hill Book Co., Inc.

### APPENDIX

#### ELECTROMAGNETIC FIELDS DUE TO A CURRENT SOURCE EMBEDDED IN A LOWER HALF-SPACE OF A TWO-LAYERED EARTH

Using the Sommerfeld integral, we can rewrite the particular solution  $\mathbf{A}^p$  [equation (12)], as

$$\mathbf{A}^p = \frac{\mathbf{J}^s}{4\pi} \int_0^\infty \frac{\lambda}{u_2} e^{-u_2|z-z'|} J_0(\lambda \rho) d\lambda, \quad (\text{A-1})$$

where  $u_i = (\lambda^2 - k_i^2)^{1/2}$  and  $\rho = [(x - x')^2 + (y - y')^2]^{1/2}$ . The horizontal wavenumber  $\lambda$  is given by  $\lambda = (k_x^2 + k_y^2)^{1/2}$ , where  $k_x$  and  $k_y$  are the wavenumbers in  $x$  and  $y$ , respectively. Using relation (Banos, 1966)

$$\iint_{-\infty}^{\infty} f(k_x^2 + k_y^2) e^{j[k_x(x-x') + k_y(y-y')] dk_x dk_y} \\ = 2\pi \int_0^{\infty} \lambda f(\lambda) J_0(\lambda \rho) d\lambda,$$

we find

$$A^p(k_x, k_y, z) = \frac{J^s}{2} \frac{e^{-u_2|z-z'|}}{u_2} \quad (A-2)$$

in Fourier transform space. The vertical components of corresponding primary fields are

$$E_z^p(k_x, k_y, z) = \frac{jk_x}{\hat{y}_2} \frac{J_x}{2} \frac{\partial}{\partial z} \frac{e^{-u_2|z-z'|}}{u_2}, \quad (A-3)$$

$$H_z^p(k_x, k_y, z) = -jk_y \frac{J_x}{2} \frac{e^{-u_2|z-z'|}}{u_2}$$

for  $J^s = i_x J_x$ , and

$$E_z^p(k_x, k_y, z) = \frac{jk_y}{\hat{y}_2} \frac{J_y}{2} \frac{\partial}{\partial z} \frac{e^{-u_2|z-z'|}}{u_2}, \quad (A-4)$$

$$H_z^p(k_x, k_y, z) = jk_x \frac{J_y}{2} \frac{e^{-u_2|z-z'|}}{u_2}$$

for  $J^s = i_y J_y$ , and

$$E_z^p(k_x, k_y, z) = \frac{\lambda^2}{\hat{y}_2} \frac{J_z}{2} \frac{e^{-u_2|z-z'|}}{u_2} \quad (A-5)$$

$$H_z^p(k_x, k_y, z) = 0$$

for  $J^s = i_z J_z$ .

In a homogeneous source-free region, the rectangular components of the vector potentials  $\mathbf{A}$  and  $\mathbf{F}$  satisfy the Helmholtz equation (Harrington, 1961, p. 129)

$$\nabla^2 \psi + k^2 \psi = 0. \quad (A-6)$$

The electric and magnetic fields due to these potentials are given by

$$\mathbf{E} = -\nabla \times \mathbf{F} - \hat{z} \mathbf{A} + \frac{1}{\hat{y}} \nabla(\nabla \cdot \mathbf{A}) \quad (A-7)$$

and

$$\mathbf{H} = \nabla \times \mathbf{A} - \hat{y} \mathbf{F} + \frac{1}{\hat{z}} \nabla(\nabla \cdot \mathbf{F}).$$

By inspection, there will be no  $E_z$  if we choose  $\mathbf{A} = 0$  and  $\mathbf{F} = i_z \theta$ . On the other hand, if we choose  $\mathbf{A} = i_z \phi$  and  $\mathbf{F} = 0$ , there will be no  $H_z$ . A field with no  $E_z$  is called transverse electric to  $z$  (TE), and a field with no  $H_z$  is called transverse magnetic to  $z$  (TM). Superposing these two independent modes, one can completely express an arbitrary field  $\mathbf{E}$  and  $\mathbf{H}$  in the source free region.

In the presence of a two-layered half-space (Figure A-1),  $\theta$  and  $\phi$  satisfy equation (A-6), and the solutions in Fourier transform space will be

$$\begin{pmatrix} \theta_i \\ \phi_i \end{pmatrix} = \begin{pmatrix} \theta_i^+ \\ \phi_i^+ \end{pmatrix} e^{-u_i z - u_i z'} + \begin{pmatrix} \theta_i^- \\ \phi_i^- \end{pmatrix} e^{u_i z - u_i z'}, \quad i = 0, 1, 2. \quad (A-8)$$

In its present coordinate system with  $z$  positive down, the superscript + denotes downgoing potential. Since there is no downgoing potential in the air,  $\theta_0^+ = \phi_0^+ = 0$ . The upgoing potentials  $\theta_2^-$  and  $\phi_2^-$  in the lower half-space are the primary terms due to

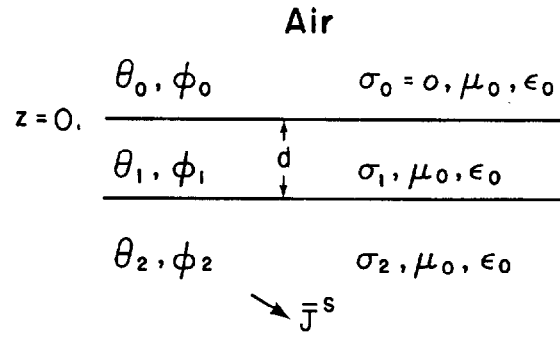


FIG. A-1. A two-layer earth with a scattering current  $J^s$  in the lower half-space.

the current element in that region. The electric and magnetic fields are then expressed in terms of  $\theta$  and  $\phi$  as

$$E_x = -\frac{\partial \theta}{\partial y} + \frac{1}{\hat{y}} \frac{\partial^2 \phi}{\partial x \partial z}, \\ E_y = \frac{\partial \theta}{\partial x} + \frac{1}{\hat{y}} \frac{\partial^2 \phi}{\partial y \partial z}, \quad (A-9) \\ E_z = -\hat{z} \phi + \frac{1}{\hat{y}} \frac{\partial^2 \phi}{\partial z^2} = \frac{\lambda^2}{\hat{y}} \phi,$$

and

$$H_x = \frac{\partial \phi}{\partial y} + \frac{1}{\hat{z}} \frac{\partial^2 \theta}{\partial x \partial z}, \\ H_y = -\frac{\partial \phi}{\partial x} + \frac{1}{\hat{z}} \frac{\partial^2 \theta}{\partial y \partial z}, \quad (A-10) \\ H_z = -\hat{y} \theta + \frac{1}{\hat{z}} \frac{\partial^2 \theta}{\partial z^2} = \frac{\lambda^2}{\hat{z}} \theta.$$

Equations (A-9) and (A-10) show that  $E_z$  depends only on  $\phi$  and  $H_z$  only on  $\theta$ . Equating the primary fields  $E_z^p$  and  $H_z^p$  given by (A-3), (A-4), and (A-5) to  $E_z$  and  $H_z$  in equations (A-9) and (A-10) with potentials  $\theta$  and  $\phi$  substituted by the upgoing primary potentials  $\theta_2^- e^{u_2 z - u_2 z'}$  and  $\phi_2^- e^{u_2 z - u_2 z'}$ , we obtain

$$\theta_2^- = -\frac{jk_y}{\lambda^2} \frac{\hat{z}_2 J_x}{2} \frac{1}{u_2}, \quad (A-11)$$

$$\phi_2^- = \frac{jk_x}{\lambda^2} \frac{J_y}{2}$$

for  $J^s = i_x J_x$ , and

$$\theta_2^- = \frac{jk_x}{\lambda^2} \frac{\hat{z}_2 J_y}{2} \frac{1}{u_2}, \quad (A-12)$$

$$\phi_2^- = \frac{jk_y}{\lambda^2} \frac{J_x}{2},$$

for  $J^s = i_y J_y$ , and

$$\theta_2^- = 0, \quad (A-13)$$

$$\phi_2^- = \frac{J_z}{2} \frac{1}{u_2},$$

for  $J^s = i_z J_z$ .

The next step is to find coefficients  $\theta_0^-$ ,  $\theta_1^+$ ,  $\theta_1^-$ , and  $\theta_2^+$  for the TE mode, and  $\phi_0^-$ ,  $\phi_1^+$ ,  $\phi_1^-$ , and  $\phi_2^+$  for the TM mode. These coefficients are determined by matching boundary conditions for tangential components of  $\mathbf{E}$  and  $\mathbf{H}$  at layer boundaries. The principle of superposition suggests that boundary conditions may be applied to each mode separately. Thus, from the boundary conditions for the TE mode, we find

$$\begin{aligned}\theta_0^- &= \frac{4N_1N_2e^{u_2d}}{(N_1+N_0)(N_2+N_1)e^{u_1d} + (N_1-N_0)(N_2-N_1)e^{-u_1d}} \theta_2^-, \\ \theta_1^+ &= \frac{2N_2(N_1-N_0)e^{u_2d}}{(N_1+N_0)(N_2+N_1)e^{u_1d} + (N_1-N_0)(N_2-N_1)e^{-u_1d}} \theta_2^-, \\ \theta_1^- &= \frac{2N_2(N_1+N_0)e^{u_2d}}{(N_1+N_0)(N_2+N_1)e^{u_1d} + (N_1-N_0)(N_2-N_1)e^{-u_1d}} \theta_2^-, \\ \text{and} \\ \theta_2^+ &= \frac{(N_1+N_0)(N_2-N_1)e^{u_1d} + (N_1-N_0)(N_2+N_1)e^{-u_1d}}{(N_1+N_0)(N_2+N_1)e^{u_1d} + (N_1-N_0)(N_2-N_1)e^{-u_1d}} \\ &\quad e^{2u_2d} \theta_2^-. \quad (\text{A-14})\end{aligned}$$

where  $d$  is the thickness of the first layer and  $N_i = (u_i/\hat{z}_i)$ . The coefficients for the TM mode have expressions identical to (A-14) with  $\theta_i$  and  $N_i$  substituted by  $\phi_i$  and  $K_i = (u_i/\hat{y}_i)$ . Replacing  $jk_x$  by  $\partial/\partial x$  and  $jk_y$  by  $\partial/\partial y$  and using equation (A-7) for  $\mathbf{E}$  and  $\mathbf{H}$ , we obtain the following electric and magnetic fields in the region of interest. Hereafter,  $\phi_i$  and  $\theta_i$  represent only the coefficient part of the potentials given by equation (A-14).

#### (a) Electric fields in the lower half-space

$$\begin{aligned}E_x^2 &= E_x^p + \frac{1}{4\pi} \int_0^\infty e^{-u_2(z+z')} d\lambda. \\ &J_x \left\{ \frac{1}{\hat{y}_2} \left[ -\frac{2(x-x')^2}{\rho^3} + \frac{1}{\rho} \right] J_1(\lambda\rho) \right. \\ &\quad \left. + \frac{(x-x')(y-y')}{\rho^2} \lambda J_0(\lambda\rho) \right\} \phi_2^+ u_2 \\ &\quad + \hat{z}_2 \left\{ \left[ \frac{2(y-y')^2}{\rho^3} - \frac{1}{\rho} \right] J_1(\lambda\rho) \right. \\ &\quad \left. - \frac{(y-y')^2}{\rho^2} \lambda J_0(\lambda\rho) \right\} \theta_2^+ \frac{1}{u_2} \\ &\quad + J_y \left\{ \frac{1}{\hat{y}_2} \left[ -\frac{2(x-x')(y-y')}{\rho^3} J_1(\lambda\rho) \right. \right. \\ &\quad \left. \left. + \frac{(x-x')^2}{\rho^2} \lambda J_0(\lambda\rho) \right] \right\} \phi_2^+ u_2 \\ &\quad + \hat{z}_2 \left[ -\frac{2(x-x')(y-y')}{\rho^3} J_1(\lambda\rho) \right.\end{aligned}$$

$$\begin{aligned}&\left. + \frac{(x-x')(y-y')}{\rho^2} \lambda J_0(\lambda\rho) \right] \theta_2^+ \frac{1}{u_2} \Big\} \\ &+ J_z \left[ \frac{1}{\hat{y}_2} \frac{(x-x')}{\rho} \lambda^2 J_1(\lambda\rho) \phi_2^+ \right].\end{aligned}$$

$$\begin{aligned}E_y^2 &= E_y^p + \frac{1}{4\pi} \int_0^\infty e^{-u_2(z+z')} d\lambda. \\ &J_x \left\{ \frac{1}{\hat{y}_2} \left[ -\frac{(x-x')(y-y')}{\rho^3} J_1(\lambda\rho) \right. \right. \\ &\quad \left. \left. + \frac{(x-x')(y-y')}{\rho^2} \lambda J_0(\lambda\rho) \right] \right\} \phi_2^+ u_2 \\ &\quad + \hat{z}_2 \left[ -\frac{(x-x')(y-y')}{\rho^3} J_1(\lambda\rho) \right. \\ &\quad \left. + \frac{(x-x')(y-y')}{\rho^2} \lambda J_0(\lambda\rho) \right] \theta_2^+ \frac{1}{u_2} \Big\} \\ &\quad + J_y \left\{ \frac{1}{\hat{y}_2} \left[ \left( -\frac{2(y-y')^2}{\rho^3} + \frac{1}{\rho} \right) J_1(\lambda\rho) \right. \right. \\ &\quad \left. \left. + \frac{(y-y')^2}{\rho^2} \lambda J_0(\lambda\rho) \right] \right\} \phi_2^+ u_2 \\ &\quad + \hat{z}_2 \left[ \left( \frac{2(x-x')^2}{\rho^3} - \frac{1}{\rho} \right) J_1(\lambda\rho) \right. \\ &\quad \left. - \frac{(x-x')^2}{\rho^2} \lambda J_0(\lambda\rho) \right] \theta_2^+ \frac{1}{u_2} \Big\} \\ &\quad + J_z \left[ \frac{1}{\hat{y}_2} \frac{(y-y')}{\rho} \lambda^2 J_1(\lambda\rho) \phi_2^+ \right].\end{aligned}$$

$$\begin{aligned}E_z^2 &= E_z^p + \frac{1}{4\pi} \int_0^\infty e^{-u_2(z+z')} d\lambda. \\ &J_x \left[ \frac{1}{\hat{y}_2} \left( -\frac{x-x'}{\rho} \right) \lambda^2 J_1(\lambda\rho) \phi_2^+ \right] \\ &\quad + J_y \left[ \frac{1}{\hat{y}_2} \left( -\frac{y-y'}{\rho} \right) \lambda^2 J_1(\lambda\rho) \phi_2^+ \right] \\ &\quad + J_z \left[ \frac{1}{\hat{y}_2} \lambda^3 J_0(\lambda\rho) \phi_2^+ \frac{1}{u_2} \right],\end{aligned} \quad (\text{A-15})$$

where the primary fields  $E_x^p$ ,  $E_y^p$ , and  $E_z^p$  are due to the primary potentials  $\theta_2^-$  and  $\phi_2^-$ . Since these potentials are identical to the primary potential  $\mathbf{A}^p$  given by equation (12), the primary electric fields may be analytically obtained using equation (13).

#### (b) Electric fields in the layer

$$\begin{aligned}E_x^1 &= \frac{1}{4\pi} \int_0^\infty e^{-u_2 z'} d\lambda. \\ &J_x \left\{ \frac{1}{\hat{y}_1} \left[ \left( -\frac{2(x-x')^2}{\rho^3} + \frac{1}{\rho} \right) J_1(\lambda\rho) \right. \right. \\ &\quad \left. \left. + \frac{(x-x')^2}{\rho^2} \lambda J_0(\lambda\rho) \right] \right\} (\phi_1^+ e^{-u_1 z} - \phi_1^- e^{u_1 z}) u_1 \\ &\quad + \frac{(x-x')^2}{\rho^2} \lambda J_0(\lambda\rho) \Big\} (\phi_1^+ e^{-u_1 z} - \phi_1^- e^{u_1 z}) u_1\end{aligned}$$

$$\begin{aligned}
& + \hat{z}_1 \left[ \left( \frac{2(y-y')^2}{\rho^3} - \frac{1}{\rho} \right) J_1(\lambda\rho) \right. \\
& \left. - \frac{(y-y')^2}{\rho^2} \lambda J_0(\lambda\rho) \right] (\theta_1^+ e^{-u_1 z} + \theta_1^- e^{u_1 z}) \frac{1}{u_2} \Big\} \\
& + J_y \left\{ \frac{1}{\hat{y}_1} \left[ - \frac{2(x-x')(y-y')}{\rho^3} J_1(\lambda\rho) \right. \right. \\
& \left. \left. + \frac{(x-x')(y-y')}{\rho^2} \lambda J_0(\lambda\rho) \right] (\phi_1^+ e^{-u_1 z} - \phi_1^- e^{u_1 z}) u_1 \right. \\
& \left. + \hat{z}_1 \left[ - \frac{2(x-x')(y-y')}{\rho^3} J_1(\lambda\rho) \right. \right. \\
& \left. \left. + \frac{(x-x')(y-y')}{\rho^2} \lambda J_0(\lambda\rho) \right] (\theta_1^+ e^{-u_1 z} + \theta_1^- e^{u_1 z}) \frac{1}{u_2} \right\} \\
& + J_z \left[ \frac{1}{\hat{y}_1} \frac{(x-x')}{\rho} \lambda^2 J_1(\lambda\rho) (\phi_1^+ e^{-u_1 z} - \phi_1^- e^{u_1 z}) \frac{u_1}{u_2} \right]. \\
E_y^1 &= \frac{1}{4\pi} \int_0^\infty e^{-u_2 z'} d\lambda. \\
J_x & \left\{ \frac{1}{\hat{y}_1} \left[ - \frac{2(x-x')(y-y')}{\rho^3} J_1(\lambda\rho) \right. \right. \\
& \left. \left. + \frac{(x-x')(y-y')}{\rho^2} \lambda J_0(\lambda\rho) \right] (\phi_1^+ e^{-u_1 z} - \phi_1^- e^{u_1 z}) u_1 \right. \\
& \left. + \hat{z}_1 \left[ - \frac{2(x-x')(y-y')}{\rho^3} J_1(\lambda\rho) \right. \right. \\
& \left. \left. + \frac{(x-x')(y-y')}{\rho^2} \lambda J_0(\lambda\rho) \right] (\theta_1^+ e^{-u_1 z} + \theta_1^- e^{u_1 z}) \frac{1}{u_2} \right\} \\
& + J_y \left\{ \frac{1}{\hat{y}_1} \left[ \left( - \frac{2(y-y')^2}{\rho^3} + \frac{1}{\rho} \right) J_1(\lambda\rho) \right. \right. \\
& \left. \left. + \frac{(y-y')^2}{\rho^2} \lambda J_0(\lambda\rho) \right] (\phi_1^+ e^{-u_1 z} - \phi_1^- e^{u_1 z}) u_1 \right. \\
& \left. + \hat{z}_1 \left[ \left( \frac{2(x-x')^2}{\rho^3} - \frac{1}{\rho} \right) J_1(\lambda\rho) \right. \right. \\
& \left. \left. - \frac{(x-x')^2}{\rho^2} \lambda J_0(\lambda\rho) \right] (\theta_1^+ e^{-u_1 z} + \theta_1^- e^{u_1 z}) \frac{1}{u_2} \right\} \\
& + J_z \left[ \frac{1}{\hat{y}_1} \frac{(y-y')}{\rho} \lambda^2 J_1(\lambda\rho) (\phi_1^+ e^{-u_1 z} - \phi_1^- e^{u_1 z}) \frac{u_1}{u_2} \right]. \\
E_z^1 &= \frac{1}{4\pi} \int_0^\infty e^{-u_2 z'} d\lambda. \\
J_x & \left[ \frac{1}{\hat{y}_1} \left( - \frac{x-x'}{\rho} \right) \lambda^2 J_1(\lambda\rho) (\phi_1^+ e^{-u_1 z} + \phi_1^- e^{u_1 z}) \right] \\
& + J_y \left[ \frac{1}{\hat{y}_1} \left( - \frac{y-y'}{\rho} \right) \lambda^2 J_1(\lambda\rho) (\phi_1^+ e^{-u_1 z} + \phi_1^- e^{u_1 z}) \right] \\
& + J_z \left[ \frac{1}{\hat{y}_1} \lambda^3 J_0(\lambda\rho) (\phi_1^+ e^{-u_1 z} + \phi_1^- e^{u_1 z}) \frac{1}{u_2} \right].
\end{aligned} \tag{A-16}$$

### (c) Magnetic fields in the air

$$\begin{aligned}
H_x^0 &= \frac{1}{4\pi} \int_0^\infty e^{u_0 z - u_2 z'} d\lambda. \\
J_x & \left\{ \left[ \frac{2(x-x')(y-y')}{\rho^3} J_1(\lambda\rho) \right. \right. \\
& \left. \left. - \frac{(x-x')(y-y')}{\rho^2} \lambda J_0(\lambda\rho) \right] \Phi_0^- \right. \\
& \left. + \left[ - \frac{2(x-x')(y-y')}{\rho^3} J_1(\lambda\rho) \right. \right. \\
& \left. \left. + \frac{(x-x')(y-y')}{\rho^2} \lambda J_0(\lambda\rho) \right] \theta_0^- \frac{u_0}{u_2} \right\} \\
& + J_y \left\{ \left[ \left( \frac{2(y-y')^2}{\rho^3} - \frac{1}{\rho} \right) J_1(\lambda\rho) \right. \right. \\
& \left. \left. - \frac{(y-y')^2}{\rho^2} \lambda J_0(\lambda\rho) \right] \Phi_0^- \right. \\
& \left. + \left[ \left( \frac{2(x-x')^2}{\rho^3} - \frac{1}{\rho} \right) J_1(\lambda\rho) \right. \right. \\
& \left. \left. - \frac{(x-x')^2}{\rho^2} \lambda J_0(\lambda\rho) \right] \theta_0^- \frac{u_0}{u_2} \right\} \\
& + J_z \left[ \left( - \frac{y-y'}{\rho} \right) \lambda^2 J_1(\lambda\rho) \Phi_0^- \frac{1}{u_2} \right]. \\
H_y^0 &= \frac{1}{4\pi} \int_0^\infty e^{u_0 z - u_2 z'} d\lambda. \\
J_x & \left\{ \left[ \left( - \frac{2(x-x')^2}{\rho^3} + \frac{1}{\rho} \right) J_1(\lambda\rho) \right. \right. \\
& \left. \left. + \frac{(x-x')^2}{\rho^2} \lambda J_0(\lambda\rho) \right] \Phi_0^- \right. \\
& \left. + \left[ \left( - \frac{2(y-y')^2}{\rho^3} + \frac{1}{\rho} \right) J_1(\lambda\rho) \right. \right. \\
& \left. \left. + \frac{(y-y')^2}{\rho^2} \lambda J_0(\lambda\rho) \right] \theta_0^- \frac{u_0}{u_2} \right\} \\
& + J_y \left\{ \left[ - \frac{2(x-x')(y-y')}{\rho^3} J_1(\lambda\rho) \right. \right. \\
& \left. \left. + \frac{(x-x')(y-y')}{\rho^2} \lambda J_0(\lambda\rho) \right] \Phi_0^- \right. \\
& \left. + \left[ \frac{2(x-x')(y-y')}{\rho^3} J_1(\lambda\rho) \right. \right. \\
& \left. \left. - \frac{(x-x')(y-y')}{\rho^2} \lambda J_0(\lambda\rho) \right] \theta_0^- \frac{u_0}{u_2} \right\} \\
& + J_z \left[ \frac{x-x'}{\rho} \lambda^2 J_1(\lambda\rho) \Phi_0^- \frac{1}{u_2} \right]. \\
H_z^0 &= \frac{1}{4\pi} \int_0^\infty e^{u_0 z - u_2 z'} d\lambda.
\end{aligned} \tag{A-17}$$

$$\begin{aligned}
& J_x \left[ \frac{y - y'}{\rho} \lambda^2 J_1(\lambda \rho) \theta_0^- \frac{1}{u_2} \right] \\
& + J_y \left[ \left( -\frac{x - x'}{\rho} \right) \lambda^2 J_1(\lambda \rho) \theta_0^- \frac{1}{u_2} \right] \\
& + J_z[0].
\end{aligned}$$

The electric and magnetic fields due to a point source of current

$\mathbf{J}^s$  can alternatively be written in a compact form as

$$\mathbf{E}(\mathbf{r}) = \mathbf{\Gamma}^E(\mathbf{r}; \mathbf{r}') \cdot \mathbf{J}^s(\mathbf{r}') \quad (\text{A-18})$$

and

$$\mathbf{H}(\mathbf{r}) = \mathbf{\Gamma}^H(\mathbf{r}; \mathbf{r}') \cdot \mathbf{J}^s(\mathbf{r}') \quad (\text{A-19})$$

where  $\mathbf{\Gamma}$  is a tensor Green's function (Harrington, 1961).